Title
Frequency-domain Green's function for a planar periodic semi-infinite phased array .I. Truncated floquet wave formulation

Journal
IEEE Transactions on Antennas and Propagation, 48(1)

ISSN
0018-926X

Authors
Capolino, F
Albani, M
Maci, S
et al.

Publication Date
2000

DOI
10.1109/8.827387

Frequency-Domain Green's Function for a Planar Periodic Semi-Infinite Phased Array—Part I: Truncated Floquet Wave Formulation

Filippo Capolino, *Member, IEEE*, Matteo Albani, *Student Member, IEEE*, Stefano Maci, *Senior Member, IEEE*, and Leopold B. Felsen, *Life Fellow, IEEE*

***Abstract*—This two-part sequence deals with the derivation and physical interpretation of a uniform high-frequency solution for the field radiated at finite distance by a planar semi-infinite phased array of parallel elementary electric dipoles. The field obtained by direct summation over the contributions from the individual radiators is restructured into a double series of wavenumber spectral integrals whose asymptotic reduction yields a series encompassing propagating and evanescent Floquet waves (FW's) together with corresponding diffracted rays, which arise from scattering of the FW at the edge of the array. The formal aspects of the solution are treated in the present paper (Part I). They involve a sequence of manipulations in the complex spectral wavenumber planes that prepare the integrands for subsequent efficient and physically incisive asymptotics based on the method of steepest descent. Different species of spectral poles define the various species of propagating and evanescent FW. Their interception by the steepest descent path (SDP) determines the variety of shadow boundaries for the edge truncated FW. The uniform asymptotic reduction of the SDP integrals, performed by the Van der Waerden procedure and yielding a variety of edge-diffracted fields, completes the formal treatment. The companion paper (Part II [1]) deals with the phenomenology of these local diffracted waves based on the present formal solution. The phenomenology encompasses all possible contributions of propagating and evanescent edge diffractions excited by propagating and evanescent FW's. The outcome is a physically appealing and accurate high-frequency algorithm, which is numerically efficient due to the rapid convergence of both the FW series and the series of relevant diffracted fields. This is demonstrated by numerical examples for radiation from a strip array in Part II.**

***Index Terms*—Floquet expansions, Green's functions, phased-array antennas.**

I. Introduction

THE electromagnetic modeling of large finite-array antennas is a subject of current interest [2], [3]. The most direct prediction approach is based on an element-by-element method of moments (MoM) implementation, which, however, becomes too complex and computationally inefficient for large-size arrays. Therefore, attention has recently been given to the efficient representation of the Green's function of the global array. When the primary objective is the input impedance of the feeding network, one can often regard the structure as infinite and employ a Floquet Wave (FW) representation of the array Green's function [4]. Accordingly, one may reduce the numerical domain of the entire array to that of a single periodic cell. These techniques fail for the near-edge elements of the array and for both near-edge and moderately far-edge elements close to scan-blindness conditions. In general, for accurate pattern design or for prediction of coupling with other antennas, the array cannot be described using the hypothesis of an infinite structure. Instead, the FW representation mentioned above needs to be modified to account for a finite array, as in several recent studies [5]–[10] dealing with frequency- and time-domain scattering from finite periodic or quasi-periodic structures. In these studies, by using the Poisson summation formula, the Green's function of a finite array is collectively represented as the radiation from a superposition of continuous truncated FW distributions over the aperture of the array. With this representation, the radiation from, or scattering by, finite phased arrays is interpreted as the radiation from a superposition of continuous equivalent FW-matched source distributions extending over the entire finite-array aperture. Asymptotically, each FW aperture distribution gives rise to an edge truncated FW plus FW-modulated edge and vertex diffracted contributions. The result can be phrased in terms of a periodicity-induced generalized geometrical theory of diffraction (GTD) ray theory, which includes nonspecular reflections as well as multiple conical edge and spherical vertex diffractions. The FW series and the series of corresponding diffracted fields converges well in those regions away from the array were all evanescent fields are negligible, thereby rendering the FW-based formulation more efficient than direct summation over the spatial contributions from each element of the array.

It may be noted that the problem of radiation from the phased array of dipoles is intimately related to the problem of plane wave scattering from an array of parallel short wire elements provided that the incident plane wave parameters are matched to the interelement phasing of the radiating array. This equivalence is made specific at appropriate places in the text.

In order to understand and quantify the high-frequency wave processes associated with FW edge diffraction, this paper deals with the canonical Green's function of a semi-infinite phased

Manuscript received April 6, 1998. This work was supported in part by the European Space Agency ESA-ESTEC, 2200 AG Noordwijk, The Netherlands, the Agenzia Spaziale Italiana (ASI). The work of L. B. Felsen was supported in part by the U.S.–Israel Binational Science Foundation, Jerusalem, Israel, under Grant 95-00399 and by ODDR&E under MURI Grants ARO DAAG55-97-1-0013 and AFOSR F49620-96-1-0028.

F. Capolino, M. Albani, and S. Maci are with the Department of Information Engineering, University of Siena, Siena, 53100 Italy.

L. B. Felsen is with the Department of Aerospace and Mechanical Engineering and Department of Electrical and Computer Engineering, Boston University, Boston, MA 02215 USA.

Publisher Item Identifier S 0018-926X(00)01280-1.

array of parallel dipoles in free space. For simplicity, the dipoles are oriented parallel to the edge truncation. (Arbitrary orientation of parallel dipoles can also be accommodated by the techniques in this paper and will be dealt with elsewhere.) The asymptotic treatment of the corner diffraction mechanisms is carried out in [11] based on a canonical Green's function for a sectoral-phased dipole array.

The high-frequency results from the present analysis and from that in [11] can be applied directly to the prediction of the radiation pattern distortion and the interantenna coupling that occurs when the actual array is placed in an electromagnetically complex environment like that of a large array in the antenna farm of a space platform (Fig. 1). Such predictions are conventionally obtained by computation-intensive tracing of ray fields from each individual element of the array through the complex environment [Fig. 1(a)]. Alternatively, global ray tracing based on the FW-modulated array aperture description permits characterization of the entire array aperture radiation in terms of a few rays whose number is independent of the number of array elements [Fig. 1(b)], thereby drastically reducing the computational effort. The same FW parametrization of rectangular phased-array Green's function asymptotics can precondition the full wave analysis of actual rectangular arrays of short wire dipoles or of apertures in an infinite ground plane as described with numerical comparisons in a forthcoming publication [12].

The presentation of this paper is divided into two parts. The present paper (Part I) deals with the mathematical formulation. The problem is first addressed by superimposing the field contributions of each source and is then transformed into FW-based spectral integrals that are evaluated asymptotically by the Van der Waerden method. Part II is devoted to the detailed physical interpretation of the variety of phenomena that arise and to the assessment of the accuracy and efficiency of the algorithm through numerical examples.

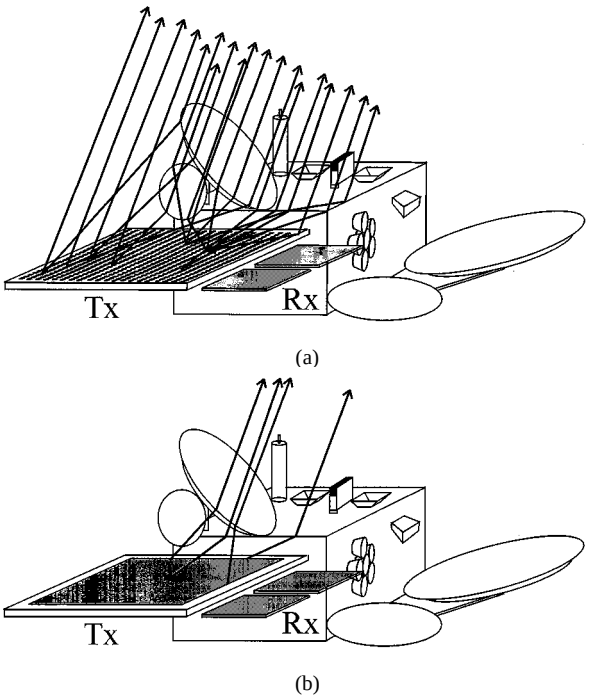

Fig. 1. (a) Element-by-element ray tracing: each array element generates a ray that must be traced through the complex environment. (b) Global ray tracing: asymptotic treatment of each FW aperture distribution for the rectangular array generates a few FW-modulated diffracted rays from the edges and vertices of the array, whose tracing through the environment yields substantial saving of computer time.

II. Formulation

The geometry of the problem is shown in Fig. 2, which comprises a phased array of infinitesimal z-directed dipoles with unit current amplitude; the array is infinite in the z-direction and semi-infinite in the x-direction. Both Cartesian and cylindrical reference coordinate systems with their z-axis along the array edge $x = 0$ are introduced so that the array occupies the region $x > 0$, $y = 0$. The interelement period is d_x and d_z in the x and z directions, respectively, and the dipoles are linearly phased with γ_x and γ_z denoting the interelement phasings along the x and z coordinates, respectively. With a suppressed time dependence $\exp(j\omega t)$, the dipole currents can be represented as

$$\vec{j}(nd_x, md_z) = \hat{z}e^{-j(\gamma_x nd_x + \gamma_z md_z)} \tag{1}$$

where $(x', z') \equiv (nd_x, md_z)$ is the position of dipole n, m; here and, henceforth, a caret $\hat{}$ denotes a unit vector and an arrow $\rightarrow$ denotes an arbitrary vector. The electromagnetic vector field at any observation point $\vec{r} \equiv (x, y, z) \equiv (\rho, \phi, z)$ can be derived from the magnetic vector potential $\vec{A}(\vec{r})$, as shown in (11). Without loss of generality, we shall restrict observations to the half-space $y > 0 (\phi \in (0, \pi))$. From symmetry, the results can be extended to directly $y < 0$. For the source array in (1),

$$\vec{A}(\vec{r}) = \sum_{m=-\infty}^{\infty} \sum_{n=0}^{\infty} g(\vec{r}; nd_x, md_z)\vec{j}(nd_x, md_z) \tag{2}$$

where g is the free-space scalar Green's function

$$g(\vec{r}; nd_x, md_z) = \frac{e^{-jk|\vec{r} - nd_x\hat{x} - md_z\hat{z}|}}{4\pi|\vec{r} - nd_x\hat{x} - md_z\hat{z}|}. \tag{3}$$

We shall employ the spectral wavenumber Fourier representation [14, p. 481]

$$g(\vec{r}; x', z') = \frac{1}{8\pi^2 j} \int_{-\infty}^{\infty} \int_{-\infty}^{\infty} \cdot \frac{e^{-j[k_x(x-x') + k_y y + k_z(z-z')]}}{k_y} dk_x\, dk_z,$$
$$k_y = \sqrt{k^2 - k_x^2 - k_z^2} \tag{4}$$

where $x' = nd_x$ and $z' = md_z$. On the top Riemann sheet of the complex k_x-plane, the branch of k_y is chosen so as to render $\Im m(k_y) < 0$ for $k^2 - k_z^2 < k_x^2$ and $k_y > 0$ for $k^2 - k_z^2 > k_x^2$. The location of branch points and branch cuts with respect to the real-axis integration path in the k_x-plane is found by introducing small losses ($\Im m(k) = 0^-$), which are eventually removed [14].

Substituting (4) into (2), a first step toward reducing the resulting formal solution involves the interchange of the sequence of the n-sum and spectral integration operations, followed by summing the resulting n-series into a closed form. Because the

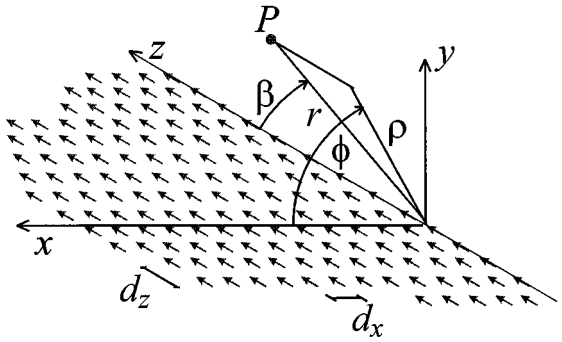

Fig. 2. Geometry of a semi-infinite array of dipoles oriented along z. The array is truncated in the x direction and infinite along the z direction.

spectral n-series summands are highly oscillatory undamped exponentials when k_x is real, the n-sum is ill behaved. For stabilization, we introduce a small shift $\epsilon > 0$ in the k_x spectrum [note that $0 < \epsilon < -\Im m(k)$], thereby ensuring uniform convergence of the n-sum along the displaced k_x-contour

$$\vec{A}(\vec{r}) = \frac{\hat{z}}{8\pi^2 j} \sum_{m=-\infty}^{\infty} \int_{-\infty}^{\infty} dk_z \int_{-\infty+j\epsilon}^{\infty+j\epsilon} dk_x \sum_{n=0}^{\infty} \cdot e^{j(k_x-\gamma_x)nd_x} e^{j(k_z-\gamma_z)md_z} \frac{e^{-j[k_x x+k_y y+k_z z]}}{k_y}. \quad (5)$$

Since $\left|e^{j(k_x-\gamma_x)d_x}\right|$ is less than unity along the integration path, the series inside the integral can be evaluated in closed form

$$\vec{A}(\vec{r}) = \frac{\hat{z}}{8\pi^2 j} \sum_{m=-\infty}^{\infty} \int_{-\infty}^{\infty} dk_z \int_{-\infty+j\epsilon}^{\infty+j\epsilon} dk_x \cdot \frac{1}{1-e^{jd_x(k_x-\gamma_x)}} e^{j(k_z-\gamma_z)md_z} \frac{e^{-j[k_x x+k_y y+k_z z]}}{k_y}. \quad (6)$$

The real poles located at

$$k_{xp} = \gamma_x + \frac{2\pi p}{d_x}, \qquad p = 0, \pm 1, \pm 2, \cdots \quad (7)$$

which define the FW wavenumbers along the x direction, are thereby placed below the k_x-integration path.

Next, we interchange the sequence of the bilaterally infinite m-series and the (k_x, k_z) spectral integration operations. The resulting spectral m-sum can be restructured via the Poisson sum formula [5], by using the identity

$$\sum_{m=-\infty}^{\infty} \exp\left[j(k_z-\gamma_z)\frac{d_z}{2\pi}\cdot 2\pi m\right] = \frac{2\pi}{d_z} \sum_{q=-\infty}^{\infty} \delta\left(k_z-\gamma_z-\frac{2\pi q}{d_z}\right) \quad (8)$$

which reduces the k_z integration to a q-series evaluated at the spectral points

$$k_{zq} = \gamma_z + \frac{2\pi q}{d_z}, \qquad q = 0, \pm 1, \pm 2, \cdots. \quad (9)$$

Equation (9) defines the FW wavenumbers along the untruncated z-domain, accounting collectively for the z-domain periodicity. The vector potential in (6) is thus reduced to

$$\vec{A}(\vec{r}) = \frac{\hat{z}}{4\pi j d_z} \sum_{q=-\infty}^{\infty} \int_{-\infty+j\epsilon}^{\infty+j\epsilon} \frac{1}{1-e^{jd_x(k_x-\gamma_x)}} \cdot \frac{e^{-j[k_x x+k_{yq} y+k_{zq} z]}}{k_{yq}} dk_x \quad (10a)$$

$$k_{yq} = \sqrt{k^2 - k_x^2 - k_{zq}^2}. \quad (10b)$$

The vector electric field generated by the dipole array is obtained from the vector potential in (10) via

$$\vec{E} = -j\omega\mu\vec{A} + \frac{1}{j\omega\epsilon} \nabla\nabla\cdot\vec{A}. \quad (11)$$

Interchanging the derivative and summation-integration operations and passing to the limit $\epsilon \to 0$ leads to the spectral representation

$$\vec{E}(\vec{r}) = \frac{1}{4\pi d_z} \sum_{q=-\infty}^{\infty} \int_{-\infty}^{\infty} \frac{\vec{G}(k_x, k_{yq}, k_{zq})}{1-e^{jd_x(k_x-\gamma_x)}} \cdot \frac{e^{-j[k_x x+k_{yq} y+k_{zq} z]}}{k_{yq}} dk_x \quad (12)$$

with the spectral vector $\vec{G}$ given by

$$\vec{G}(k_x, k_y, k_z) = \frac{\zeta}{k}\left(\hat{x}k_x k_z + \hat{y}k_y k_z + \hat{z}\left(k_z^2 - k^2\right)\right). \quad (13)$$

For arbitrary orientation of the parallel dipoles with respect to the edge, the vector in (13) is replaced by a dyadic.

Fig. 3 depicts the complex k_x-plane for the integrand in (12). We write

$$k_{\rho q} = \sqrt{k^2 - k_{zq}^2} \quad (14)$$

requiring that $\Im m(k_{\rho q}) < 0$ for $k_{zq}^2 > k^2$, and $k_{\rho q} > 0$ when $k_{zq}^2 < k^2$. This requirement is in accord with (4) and (10b), i.e., $\Im m(k_{yq}) < 0$ for $k_{\rho q}^2 < k_x^2$ and $k_{yq} > 0$ for $k_{\rho q}^2 > k_x^2$. The integration path is indented in the clockwise direction around the poles. The residues at these poles describe the FW's on the infinite array. When $k_{\rho q}$ is real ($k_{zq}^2 < k^2$), the poles located on the proper Riemann sheet ($\Im m(k_{yq}) < 0$) inside or outside the interval $(-k_{\rho q}, k_{\rho q})$ are associated with proper propagating or evanescent FW's, respectively. However, when $k_{\rho q}$ is imaginary ($k_{zq}^2 > k^2$), all the corresponding FW's are evanescent. In both cases, improper poles, which yield FW's that grow along the positive y-axis, are located on the improper Rieman sheet $\Im m(k_{yq}) > 0$; although these latter poles are not intercepted in subsequent contour deformation, their presence can affect the k_x-integration and will be accounted for in the asymptotic evaluation carried out in Section III.

To simplify the integrand in (12), we introduce the change of variables from the Cartesian (k_x, k_{yq}) to the cylindrical polar $(k_{\rho q}, \alpha)$ coordinates in the spectral domain

$$k_x = k_{\rho q}\cos\alpha, \qquad k_{yq} = k_{\rho q}\sin\alpha. \quad (15)$$

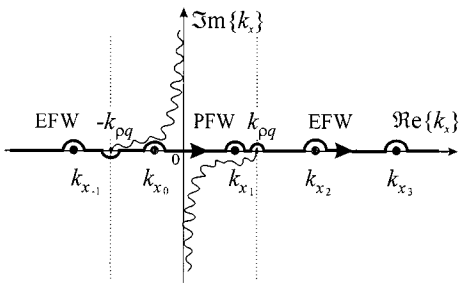

Fig. 3. Topology of the k_x-plane for each term of the q-sum in (12). The poles k_{xp} are located below the integration path; branch points occur at $k_x = \pm k_{\rho q}$, with $k_{\rho q} = \sqrt{k^2 - k_{zq}^2}$. When $|k_{zq}| > k$, the branch points $\pm k_{\rho q}$ are located on the imaginary axis.

Representing the physical coordinates (x, y, z) in terms of the polar coordinates (ρ, ϕ, z), with $x = \rho \cos \phi$, $y = \rho \sin \phi$ ($\phi \in (0, \pi)$, see Fig. 2), (12) becomes

$$\vec{E}(\vec{r}) = \frac{1}{4\pi d_z} \sum_{q=-\infty}^{\infty} \int_{C_\alpha} \vec{D}_q(\alpha) e^{-j[k_{\rho q}\rho \cos(\alpha - \phi) + k_{zq} z]}\, d\alpha \tag{16}$$

in which α is the angular spectrum variable and

$$\vec{D}_q(\alpha) = \frac{\vec{G}(k_{\rho q} \cos \alpha,\, k_{\rho q} \sin \alpha,\, k_{zq})}{1 - e^{jd_x[k_{\rho q} \cos \alpha - \gamma_x]}}. \tag{17}$$

The integration path C_α in the complex α-plane corresponds to the real axis in the k_x-plane. In particular, $C_\alpha \equiv (-j\infty, \pi + j\infty)$ is shown in Fig. 4(a) when $k_{\rho q}$ is real and $C_\alpha \equiv (\pi/2 - j\infty, \pi/2 + j\infty)$ is shown in Fig. 4(b) when $k_{\rho q}$ is imaginary. The poles α_{pq} of the function $\vec{D}_q(\alpha)$ are depicted in Fig. 4 and occur at $\alpha = \alpha_{pq}$, with

$$\alpha_{pq} = \cos^{-1}\left(\frac{\gamma_x + 2\pi p/d_x}{k_{\rho q}}\right) = \cos^{-1}\left(\frac{k_{xp}}{k_{\rho q}}\right) \tag{18}$$

here $k_{\rho q} = \sqrt{k^2 - k_{zq}^2}$ may assume real or imaginary values. The $\cos^{-1}$ function in (18) is defined through its principal values [see also Appendix A, (38) and (39)] so that the poles α_{pq} are located as depicted in Fig. 4(a) and (b) for real and imaginary $k_{\rho q}$, respectively. The integration contour C_α avoids the poles via a semicircular detour in the counterclockwise direction. The improper (nonphysical) poles are distributed along locii identical with C_α except for a translation of $\pm\pi$; these poles correspond to those on the improper Rieman sheet of the k_x plane.

The poles represent the angular spectra of FW's on the infinite array of dipoles. Poles with $k_{xp}^2 + k_{zq}^2 < k^2$ are associated with propagating Floquet waves (PFW's) (real k_{ypq}) while all other poles are associated with evanescent Floquet waves (EFW's) (imaginary k_{ypq}). From (10b) and (18)

$$k_{ypq} = \sqrt{k^2 - k_{xp}^2 - k_{zq}^2} = k_{\rho q} \sin \alpha_{pq} \tag{19}$$

with the branch of the square root defined in accord with (4): $\Im m(k_{ypq}) < 0$ when $k_{xp}^2 + k_{zq}^2 > k^2$ and $k_{ypq} > 0$ when $k_{xp}^2 + k_{zq}^2 < k^2$. For PFW, α_{pq} is real and the wave vector

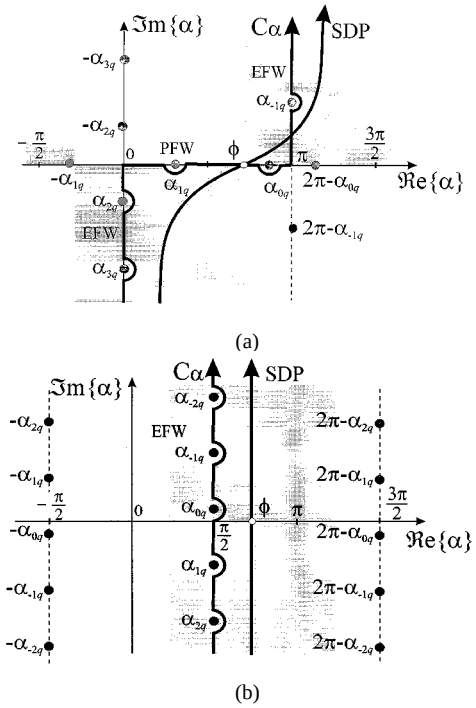

Fig. 4. Topology of the α-plane (A2), integration paths C_α, and SDP's for (a) real values of $k_{\rho q}$ and (b) imaginary values of $k_{\rho q}$. In the shaded zones, the integrand in (A2) tends to zero for large values of the imaginary part of α. The poles in the nonshaded region are improper FW poles of the k_x plane.

$\vec{k}_{pq} = (k_{xp}, k_{ypq}, k_{zq})$ associated with FW$_{pq}$ is oriented parallel to the plane $\phi = \alpha_{pq}$ in the edge-centered polar coordinate system (see Fig. 2). The plane $\phi = \alpha_{pq}$ truncates the domain of existence of the PFW$_{pq}$ on the semi-infinite array and it therefore constitutes the PFW$_{pq}$ shadow boundary. More will be said about this later.

It is worth noting that in the array *scattering* problem, when dealing with propagating FW's for which α_{pq} is real, $\pi - \alpha_{pq}$ defines the direction of incidence of that plane wave which generates by phase matching the same specular reflected field as the radiated PFW$_{pq}$; it therefore defines as well the shadow boundary for the *reflected* PFW$_{pq}$ in the scattering problem when the array is truncated.

III. High-Frequency Solution

To evaluate each integral in (16) in the high-frequency range, the integration contour is deformed into the steepest descent path (SDP) through its pertinent saddle point in the phase function

$$\alpha = \phi. \tag{20}$$

Two cases have to be distinguished depending on whether $k_{\rho q}$ is real or imaginary. Referring to Appendix A, when $k_{\rho q}$ is real the SDP assumes the conventional shape shown in Fig. 4(a), while when $k_{\rho q}$ is imaginary, the SDP is a straight line parallel to the imaginary axis [Fig. 4(b)]. In the latter case, all poles are captured during the deformation when $\phi < \pi/2$ and none is captured when $\phi > \pi/2$. The residue contributions due to the intercepted poles yield FW fields (Section III-A). The saddle-

point evaluation of the integrals along the SDP yields diffracted FW's emanating from the edge of the array (Section III-B).

A. Truncated Floquet Waves

Implementing the contour deformation described above, the electric vector field in (16) is expressed in terms of two contributions

$$\vec{E}(\vec{r}) = \sum_{p,\,q=-\infty}^{\infty} \vec{E}_{pq}^{FW}(\vec{r}) U\left(\phi_{pq}^{SB} - \phi\right) + \sum_{q=-\infty}^{\infty} \vec{E}_{q}^{d}(\vec{r}) \quad (21)$$

where

$$\vec{E}_{pq}^{FW}(\vec{r}) = \frac{1}{2d_x d_z\, k_{ypq}} \vec{G}(k_{xp},\, k_{ypq},\, k_{zq}) \cdot e^{-j(k_{xp}x + k_{zq}z + k_{ypq}y)} \quad (22)$$

arises from the residues at the poles intercepted during the path deformation and $\vec{E}_q^d(\vec{r})$ represents the integral along the SDP

$$\vec{E}_q^d(\vec{r}) = \frac{1}{4\pi d_z} \int_{\mathrm{SDP}} \vec{D}_q(\alpha) e^{-j[k_{\rho q}\rho\, \cos(\alpha-\phi) + k_{zq}z]}\, d\alpha. \quad (23)$$

As noted earlier, the residue contributions represent the FW's of the doubly infinite array; they are truncated in (21) by the Heavyside unit step function $U(\eta) = 0$ or 1 for $\eta < 0$ or $\eta > 0$, respectively, which terminates their domain of existence at the shadow boundary planes $\phi = \phi_{pq}^{SB}$. The shadow boundary is defined to occur at that angle ϕ_{pq}^{SB} for which the pole α_{pq} lies on the SDP. Expressions for ϕ_{pq}^{SB} pertaining to the various FW species, derived in Appendix A are as follows:

$$\phi_{pq}^{SB} = \alpha_{pq} = \cos^{-1}\left(\frac{k_{xp}}{k_{\rho q}}\right) \text{ for real } k_{ypq}(PFW) \quad (24a)$$

$$\phi_{pq}^{SB} = \cos^{-1}\left(\frac{k_{\rho q}}{k_{xp}}\right) \text{ for imaginary } k_{ypq}(EFW) \text{ and real } k_{\rho q} \quad (24b)$$

$$\phi_{pq}^{SB} = \frac{\pi}{2} \text{ for imaginary } k_{ypq}(EFW) \text{ and imaginary } k_{\rho q}. \quad (24c)$$

Note that the above formulation applies to $\phi \in (0,\, \pi)$; expressions relevant to $\phi \in (\pi,\, 2\pi)$ here and in what follows may be obtained by formally substituting $\phi \to 2\pi - \phi$ and $y \to -y$, $\hat{y} \to -\hat{y}$.

B. Diffracted Waves—Uniform Asymptotic Evaluation

The SDP integral in (23), which represents the $\vec{E}_q^d(\vec{r})$ contribution to the total electric field $\vec{E}$, is here broadly referred to as the diffracted field. It serves two principal functions:

1) To introduce an FW-modulated edge-diffracted q-indexed wave species, which is essentially cylindrical with respect to the array edge along the z-axis. This wave species exists for all observation angles ϕ, in contrast to the $(p,\, q)$-indexed truncated FW's in (21), which behave like plane waves [see (22)] in the region $\phi < \phi_{pq}^{SB}$ and vanish when $\phi > \phi_{pq}^{SB}$.
2) To provide the required continuity of the $\vec{E}_{pq}$ and $\vec{H}_{pq}$ fields across the ϕ_{pq}^{SB} shadow boundary of FW$_{pq}$. These analytic and physical attributes of the diffracted field will be substantiated from the asymptotic evaluation of the SDP integral in (23), which is performed next and which is interpreted in detail in Part II [1].

Anticipating briefly, the asymptotic edge diffracted field is found to be modulated by the z-domain q-indexed FW periodicity [see (9)] but, for a given q, is not affected by the x-domain p-indexed FW periodicity. The diffracted field ray vectors $\vec{k}_q^d$ are centered on the z-axis and reach the observer along diffraction cones, which are FW-modulated generalizations of the smooth-edge version in conventional GTD.

The asymptotic evaluation of the SDP integral, which defines $\vec{E}_q^d(\vec{r})$, is performed via the Van der Waerden (VdW) method [15] (see also [14, Sec. 4.4]). The asymptotics is dominated by the saddle-point contribution, but is sensitive to whether the pole is near the SDP and/or is crossed by the SDP. If the pole and the SDP are distinct, each can be evaluated separately from the other. When the SDP and pole are contiguous, the asymptotics must be refined, i.e., made uniform, to account simultaneously for both; this is the transition region near and across the FW$_{pq}$ shadow boundary ϕ_{pq}^{SB} in physical space. The VdW method proceeds by mapping the given spectral integral onto a canonical integral, which expresses the pole-SDP interaction in the simplest possible manner in addition to a regular pole-less remainder integral. The canonical integral is the error function, the transition function familiar in the uniform theory of diffraction (UTD) [16]. While there are various asymptotic techniques which yield the decomposition into the transition function plus a regular remainder, we regard the VdW method as the "cleanest" for asymptotic book keeping and best suited for our purposes. Via the VdW method, each pole is individually extracted from the spectral integrand, thereby isolating the pole contribution from the resulting regularizing remainder. Because the regularization process is addition and subtraction, the integrity of each operation is evident and its asymptotic behavior with respect to large k (i.e., high frequencies) can be assessed systematically.

Turning now to our spectral integral in (23), we have found it convenient to isolate from the spectral integrand the function [9]

$$\vec{W}_q(\alpha) = \sum_{p=-P}^{P} \left(\vec{w}_{pq-}(\alpha) + \epsilon_p \vec{w}_{pq+}(\alpha)\right), \quad \epsilon_p = \mathrm{sgn}(k_{xp}) \quad (25)$$

where

$$\vec{w}_{pq\mp}(\alpha) = \frac{-1}{2jk_{ypq}d_x} \frac{\vec{G}(k_{xp},\, \pm k_{ypq},\, k_{zq})}{\sin\dfrac{\alpha_{pq} \mp \alpha}{2}}. \quad (26)$$

In the modified remainder, this function is subtracted from $\vec{D}_q(\alpha)$ in (16). The function $\vec{W}_q(\alpha)$ is constructed in such a way as to have the same poles and residues as $\vec{D}_q(\alpha)$ in (17). As shown in Appendix B, $\vec{W}_q(\alpha)\exp(-jk_{\rho q}\rho\, \cos(\alpha-\phi))$ can be expressed in a closed analytic form on the SDP. Increasing the number P of extracted poles augments the region around the saddle point in which the function $\vec{D}_q(\alpha) - \vec{W}_q(\alpha)$ is smooth and regular, thus legitimizing its approximation by

the value it assumes at the saddle point. Note that the poles to be extracted include not only those associated with physical PFW and EFW, but also those associated with improper waves whose presence may influence the behavior of the integrand. In particular, $w_{pq+}(\alpha)$ contains the improper poles. The overall procedure, which is summarized in Appendix B, leads to the following asymptotic expression for the diffracted field

$$\vec{E}_q^d(\vec{r}) \sim \frac{1}{4\pi d_z}\sqrt{\frac{2\pi j}{k_{\rho q}\rho}}\, e^{-j(k_{\rho q}\rho + k_{zq}z)} \cdot \left[\vec{T}_q(\phi) + \sum_{p=-P}^{P} \vec{w}_{pq-}(\phi) F(\delta_{pq-}^2) + \epsilon_p \vec{w}_{pq+}(\phi) F(\delta_{pq+}^2)\right] \tag{27}$$

in which $\vec{T}_q(\alpha) = \vec{D}_q(\alpha) - \vec{W}_q(\alpha)$. This expression may be rearranged as

$$\vec{E}_q^d(\vec{r}) \sim \frac{1}{4\pi d_z}\sqrt{\frac{2\pi j}{k_{\rho q}\rho}}\, e^{-j(k_{\rho q}\rho + k_{zq}z)} \cdot \left[\vec{D}_q(\phi) + \sum_{p=-P}^{P} \left(\vec{w}_{pq-}(\phi)[F(\delta_{pq-}^2) - 1] + \epsilon_p \vec{w}_{pq+}(\phi)[F(\delta_{pq+}^2) - 1]\right)\right]. \tag{28}$$

In (25)–(28), $k_{\rho q}$ is defined in (14) and P denotes the number of poles extracted in the VdW procedure. The error function F is the transition function of the UTD [16]

$$F(x) = 2j\sqrt{x}\, e^{jx} \int_{\sqrt{x}}^{\infty} e^{-jt^2}\, dt, \text{ with } -\frac{3\pi}{2} < \arg(x) \le \frac{\pi}{2} \tag{29}$$

whose arguments $\delta_{pq\pm}^2$ in (27) and (28) are given by

$$\delta_{pq\pm} = \sqrt{2k_{\rho q}\rho}\, \sin\left(\frac{\alpha_{pq} \pm \phi}{2}\right). \tag{30}$$

The function $F(x)$ tends to unity for large magnitude of its complex argument, i.e., for observation points far from the shadow boundaries. Consequently, (28) is suitable for interpretation of the asymptotic behavior of the diffracted fields far from the shadow boundaries. For large F, the quantity $1-F$ is of asymptotic order $(k_{\rho q}\rho)^{-1}$ so that the dominant asymptotic term is associated with the FW-modulated diffraction coefficient $\vec{D}_q(\phi)$ in (17); the diffracted field has the cylindrical decay rate $\rho^{-1/2}$.

Equation (27) is more suitable for exploring the field behavior close to one of the shadow boundaries; in this case, the term associated with ϕ_{pq}^{SB} closest to ϕ becomes asymptotically dominant and necessitates the compensation of the shadow boundary discontinuity in both the truncated propagating and evanescent Floquet waves. To show this, it is convenient relate F to the complementary error function

$$\operatorname{erfc}(z) = \frac{2}{\sqrt{\pi}} \int_z^{\infty} e^{-\tau^2}\, d\tau \tag{31}$$

as follows [17]:

$$F(\delta^2) = \pm\sqrt{\pi}\, e^{j\pi/4}\delta\, e^{j\delta^2} \operatorname{erfc}(\pm e^{j\pi/4}\delta) \tag{32}$$

where the upper/lower signs apply for $\Re(e^{j\pi/4}\delta) \gtrless 0$. Equation (32) can also be written as

$$F(\delta^2) = \sqrt{\pi}\, e^{j\pi/4}\delta e^{i\delta^2} \cdot \left[\operatorname{erfc}(e^{j\pi/4}\delta) - 2U\left(-\Re e(e^{j\pi/4}\delta)\right)\right]. \tag{33}$$

As seen from (33), the function $Q(\delta_{pq-}) \equiv F(\delta_{pq-}^2)/\delta_{pq-}$, which is proportional to the term $\vec{w}_{pq-}(\phi)F(\delta_{pq-}^2)$ in (27), is discontinuous when $\Re e(e^{j\pi/4}\delta_{pq-})$ changes signs. From (31) and (33), it also follows that $\vec{w}_{pq-}(\phi)F(\delta_{pq-}^2)$ is discontinuous when its complex argument δ_{pq-}^2 crosses the imaginary axis. Taking into account that $k_{\rho q} = |k_{\rho q}|$ or $k_{\rho q} = -j|k_{\rho q}|$, when $|k_{zq}| \le k$ or $|k_{zq}| > k$, respectively, it is straightforward to verify that this discontinuity occurs exactly on the shadow boundary $\phi = \phi_{pq}^{SB}$ where the FW's are spatially truncated. The function $Q(\delta_{pq-})$ compensates uniformly for the discontinuity of the truncated FW's. Details on the compensation mechanism for the various FW species are given in Part II of this paper. Here we only mention that the terms $\epsilon_p\vec{w}_{pq+}(\phi)F(\delta_{pq+}^2)$ in (27), which correspond to improper poles in the extraction procedure, have no ϕ-discontinuity in the upper ($y > 0$) half-space region, but stabilize the asymptotic solution across the shadow boundary of a proper FW even when that boundary approaches grazing aspect.

When $|k_{zq}| > k$, the resulting diffracted field in (27) or (28) is evanescent along the ρ direction, with exponential decay $\exp(-|k_{\rho q}|\rho)$. Those radially attenuated diffracted waves that are negligible sufficiently far from the edge furnish a rough criterion for truncating the q-series of diffracted rays in (21), which is analogous to that for truncating the FW series in (21). Thus, except for field calculations very close to the array, our formulation is substantially more efficient than the ordinary element-by-element summation; this aspect will be quantified in the Part II of this paper.

IV. Summary

A uniform high-frequency solution has been presented for a semi-infinite periodic phased beam-scanning array of identical elementary dipoles oriented along the z-direction parallel to the array edge. Arbitrary orientation of parallel dipoles can also be addressed by the same formulation and will be dealt with elsewhere. The field is represented in terms of propagating (radiating) and evanescent (nonradiating) FW's and of propagating and evanescent diffracted fields, which uniformly compensate for the FW discontinuities at their shadow boundaries. The physical interpretation of the various wave processes contained in the asymptotic solution presented here is carried out in Part II of this paper, with an emphasis on the diffracted ray-field over a broad range of operating conditions. Moreover, the accuracy of the asymptotic algorithm is assessed there by numerical examples.

The present solution may be used for rectangular arrays by invoking the locality of high-frequency edge phenomena as formalized in the GTD. Accounting for the corner diffraction con-

tributions on a rectangular array via an asymptotic Green's function procedure based on the formalism here is presently under investigation [10]–[12].

APPENDIX A
THE SDP AND THE SHADOW BOUNDARIES

The SDP, for the two cases in which $k_{\rho q}$ may assume real or imaginary values, can be ascertained by decomposing the argument of the exponential term in (16) into its real and imaginary parts,

$$\begin{aligned} &-jk_{\rho q}\rho\cos(\alpha-\phi) \\ &\quad=-jk_{\rho q}\rho\,(\cos(\alpha_r-\phi)\cosh\alpha_i \\ &\qquad+j\sin(\alpha_r-\phi)\sinh\alpha_i),\ \alpha=\alpha_r+j\alpha_i. \end{aligned} \tag{34}$$

By definition, the SDP is the locus of points for which the imaginary part of the phase function in (32) is equal to that at the saddle point $\alpha=\phi$, i.e.,

$$\begin{aligned} &\Im m\left(-jk_{\rho q}\rho[\cos(\alpha_r-\phi)\cosh\alpha_i+j\sin(\alpha_r-\phi)\sinh\alpha_i]\right) \\ &\quad=\Im m(-jk_{\rho q}\rho)=\begin{cases}-k_{\rho q}\rho, & \text{for } k_{\rho q} \text{ real}\\ 0, & \text{for } k_{\rho q} \text{ imaginary.}\end{cases} \end{aligned} \tag{35}$$

Equation (33) is then reduced to

$$\begin{aligned} &\cos(\alpha_r-\phi)\cosh\alpha_i=1, && \text{for } k_{\rho q} \text{ real}\\ &\sin(\alpha_r-\phi)=0, && \text{for } k_{\rho q} \text{ imaginary} \end{aligned} \tag{36}$$

yielding the SDP depicted in Fig. 4(a) and (b), respectively.

The shadow boundary angle ϕ_{pq}^{SB} is found by imposing that the SDP passes through the pole at $\alpha=\alpha_{pq}$, i.e.,

$$\cos\left(\Re e(\alpha_{pq})-\phi_{pq}^{SB}\right)\cosh\left(\Im m(\alpha_{pq})\right)=1, \qquad \text{for } k_{\rho q} \text{ real} \tag{37a}$$

$$\sin\left(\Re e(\alpha_{pq})-\phi_{pq}^{SB}\right)=0, \qquad \text{for } k_{\rho q} \text{ imaginary.} \tag{37b}$$

Consider first a real pole α_{pq}, which is associated with a PFW; in this case, (37a) reduces to $\cos(\alpha_{pq}-\phi_{pq}^{SB})=1$ so that $\alpha_{pq}=\phi_{pq}^{SB}$, as stated in (24a). When α_{pq} is associated with an EFW ($k_{xp}^2>k_{\rho q}^2$), while maintaining $k_{\rho q}$ real, the inversion of the cos function in (18) yields

$$\alpha_{pq}=-j\cosh^{-1}(k_{xp}/k_{\rho q}), \qquad \text{for } k_{xp} \text{ positive} \tag{38a}$$

$$\alpha_{pq}=\pi+j\cosh^{-1}(k_{xp}/k_{\rho q}) \quad \text{for } k_{xp} \text{ negative} \tag{38b}$$

with positive values of $\cosh^{-1}$. In both cases, (37a) implies $\cos(\phi_{pq}^{SB})k_{xp}/k_{\rho q}=1$, from which one obtains (24b). Finally, when $k_{\rho q}$ is imaginary

$$\alpha_{pq}=\pi/2-j\sinh^{-1}(k_{xp}/|k_{\rho q}|) \tag{39}$$

and (37b) leads directly to (24c).

APPENDIX B
THE VAN DER WAERDEN PROCEDURE

Modifying $\vec{D}_q(\alpha)$ in (16) by adding and subtracting the function $\vec{W}_q(\alpha)$ defined in (25), yields

$$\vec{E}(\vec{r})=\frac{1}{4\pi d_z}\sum_{q=-\infty}^{\infty}e^{-jk_{zq}z}(\vec{I}_T+\vec{I}_W) \tag{40}$$

where

$$\vec{I}_T=\int_{\text{SDP}}\vec{T}_q(\alpha)e^{-jk_{\rho q}\rho\cos(\alpha-\phi)}\,d\alpha \tag{41}$$

$$\vec{I}_W=\int_{\text{SDP}}\vec{W}_q(\alpha)e^{-jk_{\rho q}\rho\cos(\alpha-\phi)}\,d\alpha \tag{42}$$

in which $\vec{T}_q(\alpha)=\vec{D}_q(\alpha)-\vec{W}_q(\alpha)$ is a smooth regular function in the vicinity of the SDP. Consequently, the integral in (41) can be asymptotically approximated by replacing $\vec{T}_q(\alpha)$ by its value at the saddle point $\alpha=\phi$ so that

$$\vec{I}_T\sim\vec{T}_q(\phi)\frac{\sqrt{2\pi j}}{\sqrt{k_{\rho q}\rho}}\,e^{-jk_{\rho q}\rho}. \tag{43}$$

Due to the particular choice of $\vec{W}_q$, the integral in (42) is evaluated in an exact closed form by using the equality [18]

$$\begin{aligned} &\int_{\text{SDP}}\frac{e^{-jk_{\rho q}\rho\cos(\alpha-\phi)}}{\sin\left(\dfrac{\phi_{pq}\mp\alpha}{2}\right)}\,d\alpha \\ &\quad=\frac{\sqrt{2\pi j}}{\sqrt{k_{\rho q}\rho}}\,\frac{e^{-jk_{\rho q}\rho}}{\sin\left(\dfrac{\phi_{pq}\mp\phi}{2}\right)}\,F\left(2k_{\rho q}\rho\sin^2\left(\frac{\phi_{pq}\mp\phi}{2}\right)\right) \end{aligned} \tag{44}$$

with F defined in (29). From (43) and (44), it is straightforward to obtain (27).

It is worth noting that (43) and (44) are valid for $k_{\rho q}$ real or imaginary and with corresponding SDP contours in Fig. 4(a) and (b), respectively. To reduce the left side of (44) into the standard canonical integral, use changes of variable $s=-j\sqrt{2}\sin((\alpha-\phi)/2)$ and $s=\sqrt{2}\exp(-j\pi/4)\sin((\alpha-\phi)/2)$ for $k_{\rho q}$ real and imaginary, respectively.

ACKNOWLEDGMENT

One of the authors, F. Capolino, would like to thank the Commission for Educational and Cultural Exchange between Italy and the United States for a Fulbright Grant awarded in 1997, to conduct research at Boston University, Boston, MA.

REFERENCES

[1] F. Capolino, M. Albani, S. Maci, and L. B. Felsen, "Frequency domain Green's function for a planar periodic semi-infinite phased array—Part II: Diffracted wave phenomenology," *IEEE Trans. Antennas Propogat.*, pp. 75–85, this issue.

[2] A. A. Ishimaru, R. G. Coe, G. E. Miller, and W. P. Geren, "Finite periodic approach to large scanning array problems," *IEEE Trans. Antennas Propagat.*, vol. AP–33, pp. 1213–1220, Nov. 1985.

[3] A. K. Skrivervik and J. R. Mosig, "Finite phased array of microstrip patch antennas: The infinite array approach," *IEEE Trans. Antennas Propagat.*, vol. 40, pp. 579–582, May 1992.
[4] J. R. Amitay, W. Galindo, and C. P. Wu, *Theory and Analysis of Phased Array Antennas*. New York: Wiley, 1972.
[5] L. B. Felsen and L. Carin, "Frequency and time domain bragg-modulated acoustic for truncated periodic array," *J. Acoust. Soc. Amer.*, vol. 95, no. 2, pp. 638–649, Feb. 1994.
[6] L. Carin and L. B. Felsen, "Time harmonic and transient scattering by finite periodic flat strip arrays: Hybrid (Ray)-(Floquet mode)-(MoM) algorithm," *IEEE Trans. Antennas Propagat.*, vol. 41, pp. 412–421, Apr. 1993.
[7] L. Felsen and L. Carin, "Diffraction theory of frequency- and time-domain scattering by weakly aperiodic truncated thin-wire gratings," *J. Opt. Soc. Amer.*, vol. 11, no. 4, pp. 1291–1306, Apr. 1994.
[8] L. Carin, L. B. Felsen, and T.-T. Hsu, "High-frequency fields excited by truncated arrays of nonuniformly distibuted filamentary scatterers on an infinite dielectric grounded slab: Parametrizing (leaky mode)-(Floquet mode) interaction," *IEEE Trans. Antennas Propagat.*, vol. 44, pp. 1–11, January 1996.
[9] F. Capolino, M. Albani, S. Maci, and R. Tiberio, "High-frequency analysis of an array of line sources on a truncated ground-plane," *IEEE Trans. Antennas Propagat.*, vol. 44, pp. 570–578, Apr. 1998.
[10] F. Capolino, M. Albani, A. Neto, S. Maci, and L. B. Felsen, "Vertex-diffracted Floquet waves at a corner array of dipoles," in *Int. Conf. Electromagn. Adv. Applicat. (ICEAA)*, Turin, Italy, Sept. 1997.
[11] F. Capolino, S. Maci, and L. B. Felsen, "Green's function for a planar phased sectoral array of dipoles," *Invited Paper-Radio Sci.*, ser. Special Issue 1998 URSI Int. Symp. Electromagn. Theory.
[12] S. Maci, F. Capolino, and L. B. Felsen, "Three-dimensional Green's function for truncated planar periodic dipole arrays," *Invited Paper-Wave Motion*, ser. Special Issue Electrodynamics Complex Environments.
[13] F. Capolino and S. Maci, "Uniform high-frequency description of singly, doubly, and vertex diffracted rays for a plane angular sector," *J. Electromagn. Waves Applicat.*, vol. 10, pp. 1175–1197, Oct. 1996.
[14] L. B. Felsen and N. Marcuvitz, *Radiation and Scattering of Waves*. New York: Prentice-Hall/IEEE Press, 1994.
[15] B. L. Van der Waerden, "On the method of saddle points," *Appl. Sci. Res.*, vol. B2, pp. 33–45, 1951.
[16] R. G. Kouyoumjian and P. H. Pathak, "A uniform geometrical theory of diffraction for an edge in a perfectly conducting surface," in *Proc. IEEE*, vol. 62, Nov. 1974, pp. 1448–1461.
[17] R. Rojas, "Comparison between two asymptotic methods," *IEEE Trans. Antennas Propagat.*, vol. AP–35, pp. 1489–1492, Dec. 1987.
[18] P. C. Clemmow, *Plane Wave Spectrum Representation of Electromagnetic Fields*. London, U.K.: Pergamon, 1966.

Filippo Capolino (S'94–M'97) was born in Florence, Italy, in 1967. He received the Laurea degree (*cum laude*) in electronic engineering and the Ph.D. degree, both from the University of Florence, Italy, in 1993 and 1997, respectively.

From 1994 to 1999 he was a regular teacher of antennas at the Diploma di Laurea, University of Siena, Italy, where he is currently a Research Associate. His research interests are in the areas of theoretical and applied electromagnetics, with a focus on high-frequency methods for electromagnetic scattering, and electromagnetic models of random surfaces.

Dr. Capolino was awarded the MMET'94 Student Paper Competition in 1994, the Raj Mittra Travel Grant for Young Scientists in 1996, and the "Barzilai" Prize for the best paper at the National Italian Congress of Electromagnetism (XI RiNEm) also in 1996. In 1997 he was a Fulbright Research Visitor in the Department of Aerospace and Mechanical Engineering at Boston University, Boston, MA. In 1998–1999 he continued his research at Boston University under a Grant from the Italian National Council for Research (CNR).

Matteo Albani (S'95) was born in Florence, Italy, in 1970. He received the Doctor degree (*cum laude*) in electronic engineering and the Ph.D. degree in electromagnetism, both from the University of Florence, Italy in 1998.

He is currently a Research Associate at the Information Engineering Department, University of Siena, Italy. His research interests are in the areas of theoretical and applied electromagnetics, in particular with high-frequency methods for the scattering and diffraction.

Dr. Albani received a special award for his Laura thesis work while at the University of Florence.

Stefano Maci (M'92–SM'99) was born in Rome, Italy in 1961. He received the Doctor degree in electronic engineering from the University of Florence, Italy, in 1987.

In 1990 he joined the Department of Electronic Engineering of the University of Florence, Italy, as an Assistant Professor. Since 1998 he has been and Associate Professor at the University of Siena, Italy. In 1997 he was an Invited Professor at the Technical University of Denmark, Copenhagen. Since 1996 he has been involved in projects of the European Space Agency regarding the electromagnetic modeling of antennas. His research interests are focused on electromagnetic scattering and diffraction. He also developed research activity on microwave antennas, particularly focused on the analysis, synthesis, and design of patch antennas.

Dr. Maci received the National Young Scientists "Francini" Award for his Laurea thesis in 1988 and the "Barziulai" Prize for the best paper at the National Italian Congress of Electromagnetism (XI RiNEm) in 1996. He is an Associate Editor of the TRANSACTIONS ON ELECTROMAGNETIC COMPATIBILITY.

Leopold B. Felsen (S'47–A'53–M'54–SM'55–F'62–LF'90) was born in Munich, Germany, on May 7, 1924. He received the B.E.E., M.E.E., and D.E.E. degrees from the Polytechnic Institute of Brooklyn, Brooklyn, NY, in 1948, 1950, and 1952, respectively.

In 1939, he immigrated to the United States and served in the United States Army from 1943 to 1946. After 1952 he remained with the Polytechnic (now Polytechnic University), gaining the position of University Professor in 1978. From 1974 to 1978 he was Dean of Engineering. In 1994 he resigned from the full-time Polytechnic faculty and was granted the status of University Professor Emeritus. He is now Professor of Aerospace and Mechanical Engineering, and Professor of Electrical and Computer Engineering at Boston University, Boston, MA. He is the author or coauthor of over 300 papers and author or editor of several books. He is an associate editor of several professional journals and editor of the *Wave Phenomena Series* (New York: Springer-Verlag). His research interests encompass wave propagation and diffraction in complex environments and in various disciplines, high-frequency asymptotic and short-pulse techniques, and phase-space methods with and emphasis on wave-oriented data processing and imaging.

Dr. Felsen is a member of Sigma Xi and a Fellow of the Optical Society of America and the Acoustical Society of America. He has held named Visiting Professorships and Fellowships and universities in the U.S. and abroad, including the Guggenheim in 1973 and the Humboldt Foundation Senior Scientist Award in 1981. In 1974 he was an IEEE/APS Distinguished Lecturer. He was awarded the Balthasar van der Pol Gold Medal from the International Union of Radio Science (URSI) in 1975, an honorary doctorate from the Technical University of Denmark in 1979, the IEEE Heinrich Hertz Gold Medal in 1991, three Distinguished Faculty Alumnus Awards from Polytechnic University, an IEEE Centennial Medal in 1984, and the Antennas and Propagation Society Distinguished Achievement Award in 1998. Also, awards have been bestowed on several papers authored or coauthored by him. In 1977, he was elected to the U.S. National Academy of Engineering. He has served as Vice Chairman and Chairman for both the United States and the International URSI Commission B.